Mechanical reinforcement and thermal properties of PVA tricomponent nanocomposites with chitin nanofibers and cellulose nanocrystals

Cameron W. Irvin[a,c], Chinmay C. Satam[b,c], J. Carson Meredith[b,c], Meisha L. Shofner[a,c,*]

[a] School of Materials Science and Engineering, Georgia Institute of Technology, Atlanta, GA 30332, USA
[b] School of Chemical & Biomolecular Engineering, Georgia Institute of Technology, Atlanta, GA 30332, USA
[c] Renewable Bioproducts Institute, Georgia Institute of Technology, Atlanta, GA 30332, USA

ARTICLE INFO

ABSTRACT

Investigating tricomponent materials containing poly(vinyl alcohol) (PVA), cellulose nanocrystals (CNCs), and chitin nanofibers (ChNFs) provides potential for understanding the modulation of material properties. CNCs or ChNFs in polymers have been documented previously; however, composites containing both in combination has been underexplored. The results show that at certain CNC/ChNF ratios, the modulus and tensile strength of the composites are enhanced beyond that possible with either nanofiller alone. However, composites containing CNC/ChNF ratios that corresponded to balanced nanofiller surface charges showed reduced mechanical properties, potentially due to charge-driven association of the nanofillers. Furthermore, changes in thermal degradation behavior suggested that these nanofillers could hinder initial degradation pathways, providing additional benefits to material performance. Overall, these initial results suggest that tricomponent nanocomposites utilizing PVA, CNCs, and ChNFs open additional possibilities for tuning the mechanical and thermal properties of creating high-performance materials with reduced environmental impact.

1. Introduction

Current concerns over environmental pollution and decreasing petroleum availability has generated an increasingly growing interest in biodegradable or renewable polymers and environmentally friendly materials as a whole. Renewable materials are a class of such materials derived from natural resources that continue to garner popularity and development in materials science [1–4]. Cellulose and chitin are two emerging renewable materials that are finding their way into multiple polymeric applications such as biotechnology [5,6] and packaging [7,8], often in their nanoscale forms as reinforcement material. The incorporation of renewable bioproducts into polymers offers the ability to improve their thermomechanical properties [9], change their crystalline structure [10], and help them expand into markets concerned about sustainability.

Cellulose is a biopolymer that can be derived from trees' and plants' cell walls and is among one of the most studied materials for use as a nanoscale fiber in nanocomposites. Cellulose molecules consist of repeat units of two anhydroglucose rings [11] arranged in a linear chain, forming a flat ribbon-like conformation. Groups of these long chains come together due to hydrogen bonding within the chains to form fibrils; these fibrils can be separated into individual crystals on the nanoscale that can be incorporated into polymers to enhance their overall properties [12]. These individual crystals, called cellulose nanocrystals (CNCs), are relatively inexpensive, abundant, have a low density, and have a high modulus and specific strength and have been incorporated in polymers as fillers since the mid-1990s [13], though they were isolated from cellulose structures much earlier [14,15]. Structurally, CNCs are rod-like particles with lengths of 50 to 500 nm and widths of 3 to 5 nm [11]. While they have previously been shown to be processed by extrusion in polymer matrices with sufficiently low melting temperatures such as low density poly(ethylene) [16] and poly(ethylene-co-vinyl alcohol) [17], CNCs degrade at relatively low temperatures and thus are better suited for being solution-processed in many cases [12,18]. Additionally, the sulfuric acid hydrolysis method from which many CNCs are produced leaves negatively-charged sulfonate groups on the CNC surface, which stabilize aqueous suspensions through repulsion forces but lower their thermal stability [12,19,20].

Chitin is another high molecular weight biopolymer very similar to cellulose that is found primarily in the exoskeleton/shells of arthropods such as crabs [21–23]. Chitin's chemical repeat units consist of N-acetyl-D-glucosamine, and in its nanofiber form (ChNF), chitin has been

---

* Corresponding author at: School of Materials Science and Engineering, Georgia Institute of Technology, Atlanta, GA 30332, USA.
 E-mail addresses: cirvin3@gatech.edu (C.W. Irvin), csatam3@gatech.edu (C.C. Satam), carson.meredith@chbe.gatech.edu (J. Carson Meredith), meisha.shofner@mse.gatech.edu (M.L. Shofner).

shown to be non-toxic, biocompatible, and biodegradable with potential for use as reinforcement in polymer composites [22,24]. In this nanofiber form, ChNFs possess widths of around 15 nm and lengths on the order of hundreds of nanometers, up to several micrometers [25,26]. In contrast with CNCs, ChNFs have a net positive ionic charge on their surfaces due to protonation of amine groups under sufficiently acidic conditions [21]. The opposite charges of CNCs and ChNFs make aggregation between them occur at certain weight loadings but also may be exploited as beneficial attractive forces in composites [27]. Previous use of ChNFs in nanocomposites is not nearly as well-studied as that of CNCs, however, as most research on chitinous materials appears to be focused on the water-soluble, highly-deacetylized form of chitin called chitosan [28].

Provided growing interest in using biodegradable and sustainable material alternatives, poly(vinyl alcohol) (PVA) was chosen as the polymer matrix for this study. PVA is a non-toxic, chemical resistant, and highly water-soluble synthetic polymer that can be compatible with these two nanofillers and cast into films for a variety of applications [19,21,23,28–30]. PVA is generated from the hydrolysis of poly(vinyl acetate) (PVAc) and does not exist as a singular monomer. The properties of PVA can be altered based on the molecular weight, degree of hydrolysis, and/or stereoregularity [31]. For instance, an increase in degree of hydrolysis or the molecular weight has been shown to cause a decrease in its water solubility, which can have an impact on its use in solution processing [32]. Additionally, higher molecular weight PVA has previously shown greater mechanical properties, thermal stability, and crystallinity when compared to lower molecular weight PVA [33]. In regards to PVA's use in composites, nanofillers are often added primarily as a means of improving its strength, toughness, and resistance to deformation [30]. Additionally, there is previous history of PVA thermal degradation being delayed by the introduction of nanofillers [23,34,35]. PVA has been successfully integrated with both chitin [21,36] and cellulose [9,37,38] independently and in one case in conjunction at vastly different weight loadings [39], however, the effects that the two nanofillers have at similar weight loadings in a tricomponent composite has, to the authors' knowledge, not yet been studied.

The present study evaluated the effects that the two nanofillers, CNCs and ChNFs, have on the thermomechanical properties and crystallinity of a PVA polymer matrix. In addition to comparisons of composites containing only CNCs or ChNFs, composites containing varying ratios of the two nanofillers were compared to assess the impact that differences in aspect ratio, chemical makeup, and surface charge have on properties. Lastly, the effects of polymer molecular weight on developing microstructures in these composites was assessed by comparing composites prepared by using high and low molecular weight PVA.

2. Materials and methods

2.1. Materials

Nanocomposites containing PVA, CNCs, and/or ChNFs were prepared and characterized in this work. Two PVA polymers were purchased from Sigma-Aldrich. One of the polymers had a weight average molecular weight of 31,000–50,000 g/mol and was 98–99% hydrolyzed. The other polymer had a weight average molecular weight of 146,000–186,000 g/mol and was 99 + % hydrolyzed. The polymer with the higher molecular weight is denoted in this paper as HPVA, and the polymer with the lower molecular weight is denoted as LPVA. Freeze-dried CNCs with a sulfonate content of 1 wt% were provided by the USDA US Forest Service Forest Product Laboratory in Madison, Wisconsin. CNCs were then redispersed in water at a weight loading of 5.5% in aqueous suspension. ChNFs were produced by the authors using a method previously described at a weight loading of 0.5% in aqueous suspension [26]. The precursor material used to produce the

ChNFs was Crabshell Fertilizer from Neptune's Harvest in Gloucester, Massachusetts. Glacial acetic acid was purchased from Sigma-Aldrich and used as received.

2.2. Nanocomposite solution processing procedure

PVA powder of one molecular weight (HPVA or LPVA) was mixed with deionized water at 300 RPM with a stir bar in a water bath at 100 °C until no visible PVA particles were present. The amount of PVA powder mixed was consistent at 4.75 g, but the amount of initial water it was dissolved into varied depending on the amount of nanofillers needed, which always resulted in a final loading of 5 wt% in suspension. If containing CNCs and/or ChNFs, the solution was cooled to below 50 °C and 1 mL glacial acetic acid for every 99 mL of solution was added to reduce the solution's pH and encourage dispersion of the ChNFs. The desired amount of ChNFs suspended in water at 0.5 wt% were then added to the PVA solution, and the components were mixed at 300 RPM with a stir bar for at least 30 min. Finally, the desired amount of CNCs suspended in water at 5.5 wt% was added and mixed at 300 RPM with a stir bar for at least 30 min. The resulting nanocomposite suspension was cast into a polystyrene Petri dish and covered with aluminum foil to prevent contamination during drying. For neat PVA polymer samples containing no nanofillers, PVA was dissolved in deionized water with a stir bar at 300 RPM in a 100 °C water bath. The resulting solution was cast in a polystyrene Petri dish and allowed to dry in the same fashion as the nanocomposite samples. Drying to a solid film took between 7 and 12 days depending on the water content and PVA type. In all cases studied here, the filler loading in the nanocomposites was kept constant at 5 wt%. This filler loading consisted of either only CNCs, only ChNFs, or different mixtures of CNCs and ChNFs at weight ratios of 1:4, 1:1, and 4:1. The naming convention for samples in this paper follows the template: [wt%]CNC/[wt%]ChNF/[L or H] PVA. For example, a sample containing 1 wt% CNC and 4 wt% ChNF in high molecular weight PVA is denoted as 1CNC/4ChNF/HPVA.

2.3. Polarized optical microscopy

Polarized optical microscopy (POM) was performed utilizing an Olympus BX51 microscope in bright field mode with images captured by an Olympus UC30 camera. A polarizer was applied below the sample stage at an angle 90° to the analyzer so that no light was able to propagate through the two cross polarizers. Samples were then placed on the stage and analyzed to assess nanofiller aggregation.

2.4. Titration testing and zeta-potential testing

To more fully understand the nature of nanofiller interactions in suspension and the resulting nanocomposite films, titration and zeta-potential testing was performed. For the titration testing, a 5.5 wt% aqueous suspension of CNCs was diluted with DI water to approximately 1 wt%. The resulting suspension was ion exchanged with Merck Ion Exchanger I, a strongly acidic cation exchange resin, to remove any cations. The resin was then washed with DI water to wash out entrapped CNCs and the resulting suspension was titrated against a 1.5 N NaOH solution by potentiometric titration with a Mettler Toledo Seven Excellence S400 pH meter. A 0.5 wt% aqueous ChNF suspension was ion exchanged with Alfa Aesar Amberlite IRN-78, a strongly basic anion exchange resin, to remove acetate anions. This resin was then washed with DI water to wash out entrapped ChNFs. A volume of 20 mL of 0.25 N HCl was added to the resulting suspension which was then titrated against a 0.5 N NaOH solution by potentiometric titration. Both titrations were repeated three times, and the results were reported as an average ± standard deviation.

For zeta-potential testing, a series of aqueous CNC/ChNF suspensions were prepared by mixing the 0.5 wt% ChNF and 5.5 wt% CNC aqueous suspensions to obtain different ratios of ChNF to CNC by

weight. The suspensions were diluted with acidified water that consisted of 1 mL acetic acid in 99 mL water to mimic the nanocomposite preparation conditions. Each suspension's zeta-potential was then measured using a Malvern Nano-ZS90 Zetasizer with an equilibration time of three minutes. Each reading was repeated three times, and the count averaged zeta-potential of distribution was used with the maximum-observed standard deviation of the three readings being used as the uncertainty.

2.5. FTIR characterization

Chemical structure changes were assessed using Fourier Transform Infrared Spectroscopy with an Attenuated Total Reflectance fixture (ATR-FTIR). A Thermo Fisher Scientific Nicolet iS50 FTIR spectrometer was utilized for this testing. Spectra were generated based on the average of 64 scans with a resolution of 4 cm^{-1}, then normalized to a C-H stretching peak around 2910 cm^{-1} that did not appear to shift with the introduction of nanofillers.

2.6. Thermogravimetric analysis

Thermogravimetric analysis (TGA) was conducted on the neat PVA and nanocomposite samples. A single witness sample for each of the neat PVA and nanocomposite samples with a mass ranging from 8 to 12 mg was punched from the films and dried for one hour at 110 °C, held at lab conditions for 40–48 h, and then tested with a TA Instruments TGA Q50 with platinum pans in a flowing nitrogen gas environment. The TGA protocol heated the samples from 30 to 110 °C, held them isothermally for one hour to remove residual water, then heated them at 10 °C/min up to 600 °C. Testing was performed to evaluate any effects the nanofillers might have on sample degradation and to measure sample water content.

2.7. Modulated differential scanning calorimetry

To assess the crystallinity of samples, modulated differential scanning calorimetry (MDSC) was performed utilizing a TA Instruments Discovery DSC with standard aluminum pans in a flowing nitrogen gas environment. Two of each of the neat PVA and nanocomposite samples were tested. Sample masses used were 5 mg ($\pm$ 0.5 mg). These samples were dried in an oven for one hour at 110 °C prior to testing. Samples were heated from 30 °C to 250 °C at a rate of 10 °C/min., held for five minutes at 250 °C, then cooled to 30 °C at a rate of 10 °C/min, per ASTM D3418. The modulation rate was set to 1 °C every 40 s. Enthalpy of fusion was calculated from the reversible heat flow melting peaks and compared to a 100% crystalline PVA value of 161 J/g, to obtain the percent crystallinity of the sample [40]. In order to account for nanofiller weight percentage, sample mass for this % crystallinity calculation was adjusted to consider the PVA mass only. An equation outlining this calculation is shown below, where X_c represents the sample crystallinity, ΔH_m represents the enthalpy of fusion for the sample, ΔH_m^o represents the 100% crystalline sample value, and w is the PVA weight fraction:

$$X_c = \frac{\Delta H_m}{w \Delta H_m^o}$$

2.8. Mechanical testing

Samples were cut from the films with an ASTM D-1708 die cutter and dried for one hour in an oven at 110 °C to remove water. Samples were held on the ends with the center bridge suspended in air to optimize water removal uniformly from the testing region of the sample. Samples were then kept at laboratory conditions for 40–48 h, and humidity levels in the laboratory were monitored. Humidity levels were observed to stay between 35% and 52% depending on the day of measurement.

Samples were tested following the ASTM D-1708 standard for polymer microtensile testing. An Instron 5566 Materials Testing Frame and a 1000 N load cell were used for testing tensile properties. After drying and conditioning, each sample was placed in the grips at a gage length of 22 mm. Samples' thicknesses were 0.3 mm $\pm$ 0.09 mm. The tests were conducted at a displacement rate of 0.1 mm/minute until fracture. While the microtensile testing standard is not designed to obtain quantitative Young's modulus values, the testing data were used to obtain relative modulus data. The relative modulus of the samples was calculated by taking the slope of the stress–strain curve from 5 MPa to 30 MPa for each sample. Tensile strength was indicated as the maximum stress experienced by the sample during testing. Strain at break values were calculated from the initiation point of 40% drop off in recorded force within the software. All data reported in this document is represented as an average $\pm$ standard deviation. For statistical analysis between sets, a two-tailed Student's T-Test assuming unequal variances and an alpha value of 0.05 was performed. Statistical significance was determined by having a sample set average with a p value of less than 0.05. Sample set averages that were statistically significantly greater than the neat PVA film were indicated with an * in figures, while a ˆ indicates a sample set average that is statistically significantly greater than all other values. Complete statistical maps for modulus, tensile strength, and strain at break are included in the Supporting Information (Figs. S1, S2 and S3, respectively).

3. Results and discussion

3.1. Polarized optical microscopy

Neat PVA and nanocomposite films were imaged with POM to qualitatively assess the levels of aggregation between nanofillers in each sample, and the images are displayed in Fig. 1. In the images, neat PVA films (Fig. 1a and g) possessed a consistent coloring throughout. In comparison, the 5CNC samples (Fig. 1b and h) showed white features that could be birefringence from CNCs aggregates. In contrast, the 5ChNF samples (Fig. 1f and l) showed fewer white areas and resembled the neat polymer films more closely, possibly indicating that there was less aggregation of ChNFs. The tricomponent composites (Fig. 1c–e and 1i–k) showed white features as well, and the features generally were smaller and more homogeneously distributed over the area in the images. Overall, these images indicated that some degree of nanofiller agglomeration was present in all of the nanocomposites containing CNCs. Despite the appearance of nanofiller aggregation in POM images, the neat PVA and nanocomposite films appeared transparent to the naked eye (Fig. S4).

3.2. Interactions between CNCs and ChNFs

To characterize the interactions between CNCs and ChNFs in suspension, titration and zeta-potential testing were performed. The titration tests provided surface charge values for CNC and ChNF in aqueous suspension, while the zeta-potential tests investigated how these surface charges changed when CNC and ChNF suspensions were combined. The titration experiments yielded surface charge values of 1.4 $\pm$ 0.1 meq/g and 0.49 $\pm$ 0.09 meq/g for the ChNFs and CNCs, respectively.

The resulting equivalents for ChNFs and CNCs from these tests represented the maximum number of cationic groups, primarily free amine groups for ChNFs, and, anionic groups, primarily sulfate groups for CNCs that could participate in any neutralization reactions. When CNCs and ChNFs were mixed together in suspension, the oppositely charged surface groups could interact, leading to the formation of a ChNF-CNC complex or aggregate. However, this assembly process would be dependent on the total number of free groups present, which in turn would depend on the pH of the surrounding medium and presence of ions, as governed by the screening effect. The actual aggregate
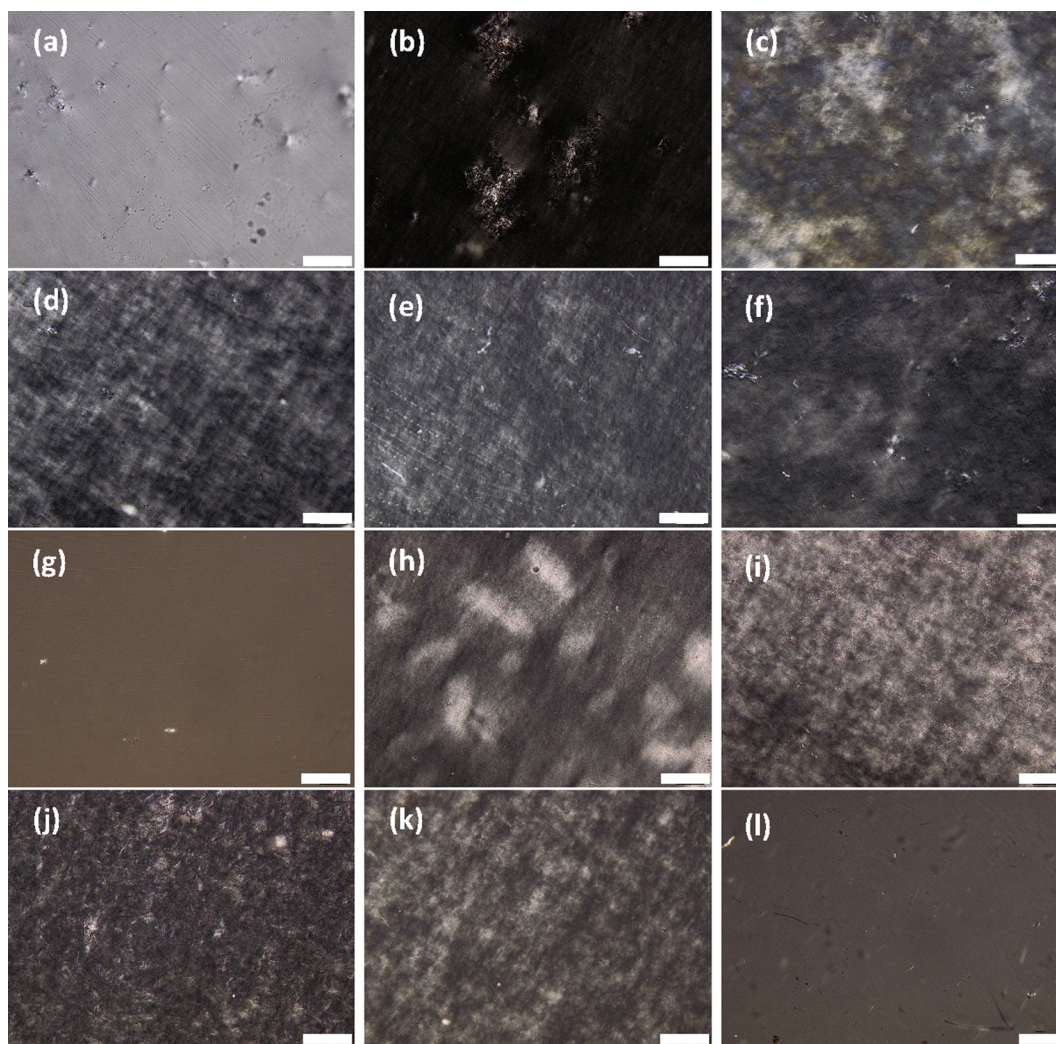
Fig. 1. Polarized optical microscopy images of (a) Neat HPVA, (b) 5CNC/HPVA, (c) 4CNC/1ChNF/HPVA, (d) 2.5CNC/2.5ChNF/HPVA, (e) 1CNC/4ChNF/HPVA, (f) 5ChNF/HPVA, (g) Neat LPVA, (h) 5CNC/LPVA, (i) 4CNC/1ChNF/LPVA, (j) 2.5CNC/2.5ChNF/LPVA, (k) 1CNC/4ChNF/LPVA, (l) 5ChNF/LPVA. Scale bars are 200 µm.
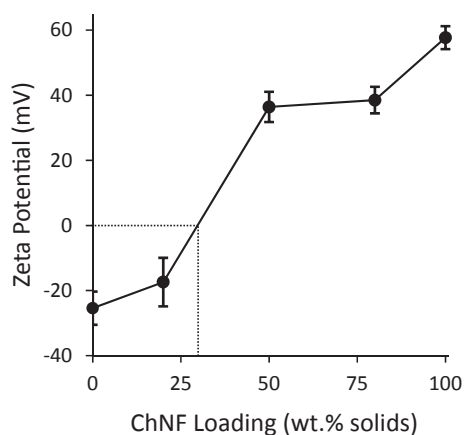

Fig. 2. Zeta Potential of CNC and ChNF suspensions at various ratios.

formation could be inferred from zeta potential measurements of various ChNF/CNC mixtures. The resulting data for these tests is shown in Fig. 2.

In CNC/ChNF mixtures, the suspensions were stabilized by strong electrostatic repulsions between oppositely charged particles. In suspensions containing CNCs and ChNFs, the zeta potential values were intermediate between those obtained for the suspensions containing only one type of nanofiller. Interpolating the data in Fig. 2 suggests that the CNCs and ChNFs neutralize one another at a CNC:ChNF mass ratio of approximately 3:1. This ratio, while approximate, is comparable to the ratio present in the 4CNC/1ChNF nanocomposites.

3.3. FTIR

ATR-FTIR analysis was performed on both HPVA and LPVA for each of the five nanofiller loaded samples and neat polymer with the aim of understanding the changes in chemical structure as a result of the introduction of CNCs and ChNFs into the system. From the spectra for HPVA represented in Fig. 3 (staggered for clarity), the large peak in the 3500–$3000 \, cm^{-1}$ range was attributed to stretching of hydrogen–bonded hydroxyl groups. Hydroxyl groups are present on PVA, CNC and ChNF, as well as any absorbed water that is present. The highest intensity peak in this range belonged to 2.5CNC/2.5ChNF/HPVA, followed by 1CNC/4ChNF/HPVA, with progressively smaller intensity peaks from 5ChNF/HPVA, 5CNC/HPVA, neat HPVA, and 4CNC/1ChNF/HPVA. Two peaks at 1720 and $1660 \, cm^{-1}$ could be attributed to C=O and C—O stretching of acetyl groups, which appeared to grow in intensity with ChNF composition, as expected. The medium sized peak at $1410 \, cm^{-1}$ was assigned to CH_2 and CH_3 bending deformation. The peaks around 1380, 1327, and $1235 \, cm^{-1}$ were
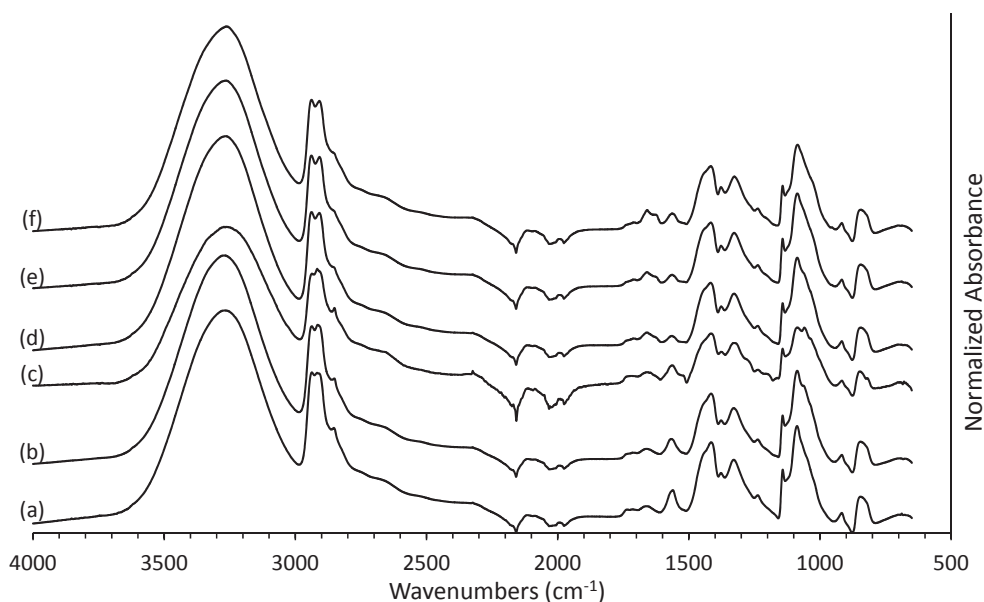
Fig. 3. FTIR analysis of (a) Neat HPVA, (b) 5CNC/HPVA, (c) 4CNC/1ChNF/HPVA, (d) 2.5CNC/2.5ChNF/HPVA, (e) 1CNC/4ChNF/HPVA, and (f) 5ChNF/HPVA.

attributed to the bending of C-H, CH_2, and -OH, while the peak around 1086 cm^{-1} was considered to be C—O stretching [41]. There is an additional peak at 1065 cm^{-1} that was only present in samples containing at least 2.5 wt% CNCs, indicating that it may be the result of alkoxy C-O-C group stretching or primary aliphatic alcohol stretching in CNCs [42]. However, despite the presence of alkoxy groups in ChNFs, this peak does not appear in the samples containing higher amounts of ChNFs. Skeletal signals appeared around the 915 and 845 cm^{-1} bands.

The spectra of LPVA represented in Fig. 4 displayed the same structural peaks discussed previously for HPVA. In regards to the differences in intensities of the hydrogen bonding peak between 3500 and 3000 cm^{-1}, the highest intensity peak belonged to 2.5CNC/2.5ChNF/LPVA, followed by 5CNC/LPVA, 5ChNF/LPVA, 1CNC/4ChNF/LPVA, 4CNC/1ChNF/LPVA, and neat LPVA. Additionally, while only 4CNC/1ChNF/HPVA and 5ChNF/HPVA experienced a small shift at this peak to higher wavenumbers compared to neat HPVA, the entirety of the

LPVA sample set experienced a 10–20 cm^{-1} shift to higher wavenumbers in comparison to neat LPVA. While the peaks were broad, a shift to lower wavenumbers is often attributed to the presence of hydrogen bonds [43,44], which suggested the addition of CNCs/ChNFs to the LPVA caused a decrease in the amount of hydrogen bonding within the system [45]. A main difference between the HPVA and LPVA sets was in regards to the 1720 cm^{-1} peak, which was much more pronounced in the LPVA sample sets. As a peak belonging to the C═O stretching of acetyl groups, the higher intensities of the LPVA analysis may have been the result of the higher amount of acetyl groups present in the slightly less hydrolyzed LPVA.

3.4. Thermal degradation

TGA was used to assess the thermal degradation patterns of the neat PVA and the nanocomposites. The analysis was used to help understand
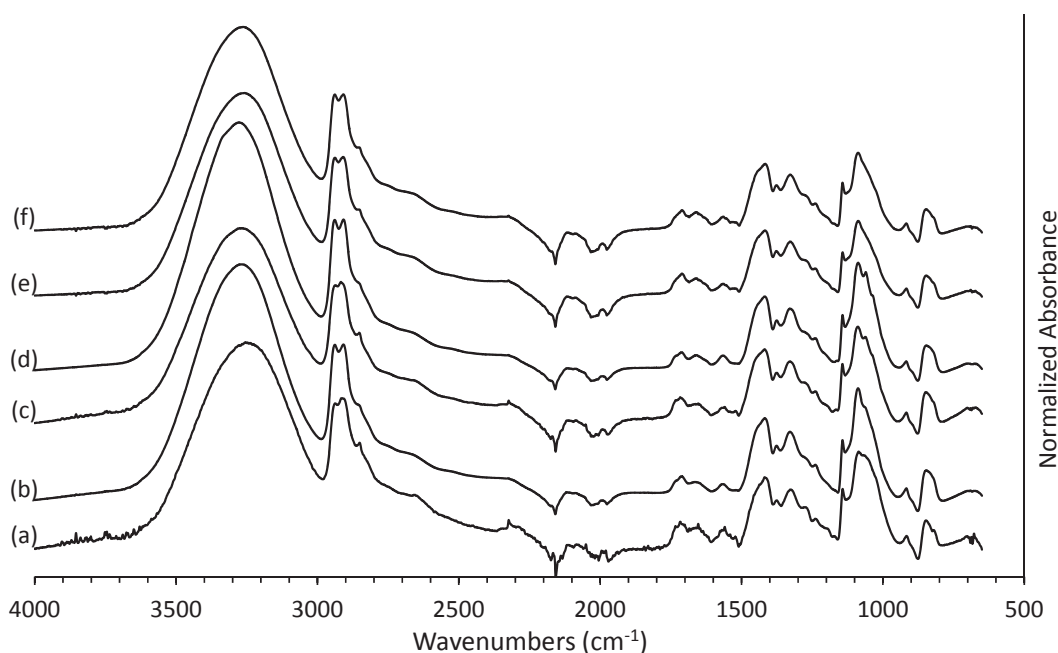

Fig. 4. FTIR analysis of (a) Neat LPVA, (b) 5CNC/LPVA, (c) 4CNC/1ChNF/LPVA, (d) 2.5CNC/2.5ChNF/LPVA, (e) 1CNC/4ChNF/LPVA, and (f) 5ChNF/LPVA.

Table 1

TGA data that provides the first and second degradation onsets and the final residual weight percentage.

Sample name	Onset degradation temperature 1 (°C)	Onset degradation temperature 2 (°C)	Residual weight (%)
Neat HPVA	241	406	7.1
5CNC/HPVA	253	400	10.3
4CNC/1ChNF/HPVA	257	400	8.5
2.5CNC/2.5ChNF/HPVA	262	429	8.9
1CNC/4ChNF/HPVA	256	423	9.4
5ChNF/HPVA	242	421	11.7
Neat LPVA	252	429	9.1
5CNC/LPVA	256	412	8.2
4CNC/1ChNF/LPVA	263	411	8.5
2.5CNC/2.5ChNF/LPVA	248	414	9.5
1CNC/4ChNF/LPVA	246	419	10.5
5ChNF/LPVA	254	423	10.5

the impact that the nanofillers had on thermal stability and whether they formed structures that were more resistant to degradation at higher temperatures. Table 1 outlines the onset of the two degradation events in addition to the residual weight percentage left in the pan at the conclusion of the test.

The samples experienced the same general thermal degradation pattern, which consisted of three weight loss steps (Figs. S5 and S6). The first weight loss occurred below 110 °C and was attributed to the loss of water in the sample. HPVA- and LPVA-based samples showed a consistent water content of approximately 3%, indicating that the drying and conditioning steps affected the samples relatively uniformly. The second weight loss step indicated the beginning of PVA degradation, and it occurred among all samples in the temperature range of 240 – 265 °C. It was also likely that CNC and ChNF degradation was occurring simultaneously at different rates within this weight loss step based on the degradation patterns for the nanofillers when not contained in a composite. CNCs utilized in this study had a degradation temperature around 189 °C and ChNFs were measured to degrade at 285 °C (Fig. S7). In comparison to the neat PVA, most of the nanocomposite samples, except the 2.5CNC/2.5ChNF/LPVA and 1CNC/4ChNF/LPVA samples, exhibited a higher onset degradation temperature for this step. This data is supported by a study performed by Sriupayo et al. [23]. This work also showed that the introduction of α-chitin whiskers caused an overall delay in thermal degradation in PVA nanocomposites compared to neat PVA. For higher weight percentages up to 25% CNCs, thermal degradation has been shown to be delayed by up to 80 °C for PVA nanocomposites compared to neat PVA [35]. In another study for PVA and silica nanocomposites, the initial onset of degradation temperature was higher in the nanocomposites than in neat PVA. Additionally, using mass spectrometry, they were able to identify that polyene structures are formed during the first degradation step through dehydration [34]. However, this behavior is not general and

depends on component interactions and the degradation temperature of the neat polymer. In a study regarding poly(lactic acid) (PLA) composites with cellulose whiskers, the nanocomposites were shown to degrade at a lower temperature compared to the neat PLA [46]. Lastly, Pracella et al. (2014) showed similar results of earlier degradation in non-PVA systems in a study with PLA, PVAc, and CNCs with neat PVAc beginning degradation first, followed by pure CNCs, 1 wt% CNC/PLA, 1 wt% CNC/PVAc/PLA, and neat PLA [47].

The second major weight loss step, which occurred in the range of 400–430 °C. This has been previously attributed to chain-scission reactions and resulted in products of acetaldehyde, low-molecular-weight polyenes, benzenoid derivatives, furan, acetone and acetic acid [34]. LPVA-based samples showed that there was a progressively increased delay in this degradation step as the amount of CNCs was reduced in the composite, but all composites exhibited this degradation step at a lower onset temperature than the neat LPVA. The HPVA samples did not show the same trend, but the two lowest onset degradation temperatures for this process belonged to witness samples cut from the 5CNC and 4CNC/1ChNF films. This result could be related to the lower degradation temperature of CNCs in comparison to ChNFs. Outside of these two similarities, no trend related the behaviors of the HPVA- and LPVA-based samples. In regards to the residual solids found at the conclusion of each test, the values were not greatly different from one another (Table 1). and did not show any clear trends.

3.5. Matrix crystallinity

MDSC was used to assess the relative crystallinity values of each of the films in order to more completely understand the effects of filler addition on matrix crystallinity. The use of MDSC allowed the total heat flow to be split into its reversible and non-reversible parts. Given PVA's propensity for thermally degrading near its melting point due to the

Table 2

MDSC data for HPVA- and LPVA- based samples.

Sample name	Melting temperature (°C)	Enthalpy of fusion (J/g)	Crystallinity (%)
Neat HPVA	211 ± 3	61 ± 0	38 ± 0
5CNC/HPVA	200 ± 0	68 ± 0	44 ± 0
4CNC/1ChNF/HPVA	199 ± 8	39 ± 9	25 ± 5
2.5CNC/2.5ChNF/HPVA	198 ± 0	49 ± 1	32 ± 1
1CNC/4ChNF/HPVA	200 ± 3	45 ± 7	29 ± 5
5ChNF/HPVA	200 ± 0	40 ± 10	27 ± 6
Neat LPVA	200 ± 8	41 ± 3	25 ± 2
5CNC/LPVA	200 ± 2	52 ± 8	34 ± 5
4CNC/1ChNF/LPVA	187 ± 1	48 ± 4	31 ± 3
2.5CNC/2.5ChNF/LPVA	188 ± 2	51 ± 2	33 ± 1
1CNC/4ChNF/LPVA	190 ± 3	38 ± 4	25 ± 2
5ChNF/LPVA	184 ± 1	49 ± 6	32 ± 3

production of volatile products and overall dehydration above 200 °C [48], this calorimetry method allowed for the degradation and melting to be separated [49], likely leading to a more accurate measurement of crystallinity. Additionally, only data obtained during the first heating ramp were analyzed since the data obtained from a second heating step would likely be affected more strongly by polymer degradation (example heat flow curves are given in Figs. S8 and S9). Table 2 displays the melting temperature, enthalpy of fusion, and % crystallinity values taken from the reversible heat flow signal during melting.

The addition of CNCs and ChNFs affected the crystal structure and crystallinity of both PVA matrices. The crystal structure was assessed qualitatively through measuring the melting temperature. If there is no change to the crystal form, changes in melting temperature can be used to qualitatively understand the size of crystalline domains and/or the level of crystal perfection. Lower melting temperatures, such as those observed here, are associated with smaller, less perfect crystalline domains. The majority of the composites showed lower melting temperatures than the neat polymer, and that decrease in melting temperature was up to 10 °C. The one notable exception to this behavior was the 5CNC/LPVA composite, which had an average melting temperature that was equal to that of the neat LPVA. A lowered melting temperature with nanocellulose addition has been observed previously for nanocellulose/PVA composites, and this trend was more likely to be observed in PVA polymers with very high levels of hydrolysis, though the melting temperature depression observed in that work was lower than that seen here [9]. Melting temperature depression of PVA with a high level of hydrolysis was also observed for montmorillonite/PVA composites with similar filler loadings. Montmorillonite platelets should have the ability to form hydrogen bonds with PVA. Additionally, as loadings increased, the composites with montmorillonite had progressively lower melting temperatures [50].

For the composites made with HPVA, the crystallinity was increased in the 5CNC composite, but the other composite samples showed lower values of crystallinity. This trend suggested that the CNCs and ChNFs interacted differently with the HPVA. Both types of nanofillers had hydroxyl groups on their surfaces which could form hydrogen bonds with PVA; however, they each had different surface charges associated with other features than the hydroxyl groups. The ChNFs contained protonated amine groups, leading to a net positive surface charge, and the CNCs had sulfate ester groups. These groups, which were produced during hydrolysis with sulfuric acid, result in a net negative CNC surface charge. The presence of these different groups, hydroxyls and charged groups, could affect the crystallization of PVA.

Hydrogen bonding between ChNFs and PVA [23,39,45] as well as between CNCs and PVA [30,38,41] has been reported in previous studies with nanocomposites and may be present in this study as well. Results for polymer blends containing PVA and polymeric chitin, i.e. not in nanofiber form, have shown that the polymers interact strongly through hydrogen bonding, leading to reductions in crystallinity of both components [45]. While polymeric chitin could interact differently with PVA than ChNFs, this reported behavior in addition to the observation that all the HPVA composites containing ChNFs had lowered matrix crystallinity, it is likely that interactions between ChNFs and HPVA reduced crystallinity.

Though PVA is largely an uncharged and nonionic polymer, it has previously been used in metal ion removal through electrostatic interactions with cations, including Ag^+ [51], $Fe(III)^{3+}$ [52], and Cu^{2+} [53]. The ionic bonding required for removal occurs as cations bind to the -OH groups of the PVA, which may also be interacting with the protonated amine groups on the ChNF in our system. Additionally, while sulfate groups have previously been shown to bind to PVA [54], the low amount of sulfate groups present on the CNC's (approximately 1 wt%) would suggest they do not experience as much electrostatic binding as the ChNF that possesses much more amine binding sites. Therefore, while the amount of hydrogen bonding was found to be relatively the same between 5CNC/PVA and 5ChNF/PVA, the presence
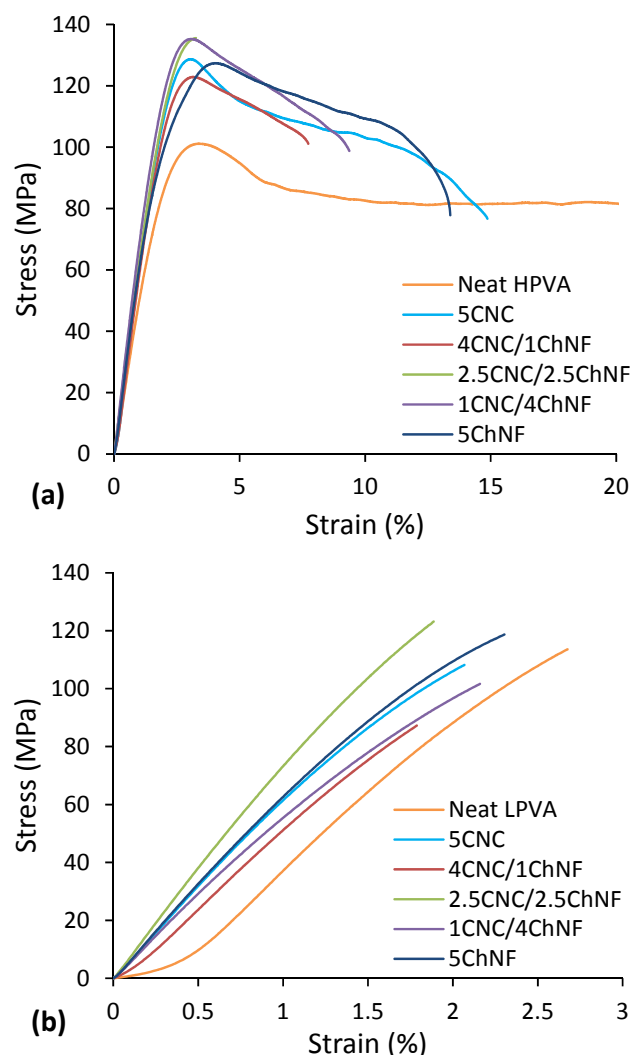
Fig. 5. Representative stress-strain curves of (a) HPVA-based samples and (b) LPVA-based samples. (For interpretation of the references to colour in this figure legend, the reader is referred to the web version of this article.)

of greater electrostatic bonding for bi- and tricomponent composites containing ChNF could be a differentiating factor in greater overall filler/matrix interactions and, thus, a decrease in polymer crystallinity [9].

The LPVA-based samples showed a different trend in crystallinity with the addition of nanofibers. With the exception of the 1CNC/4ChNF/LPVA composite, all LPVA composites possessed higher levels of crystallinity than the neat LPVA. The crystallinity values for these composites were not distinct due to the experimental error. The melting temperatures for the composites containing ChNFs were lower than those for the neat LPVA and 5CNC composite, this trend suggested that the crystals were smaller and/or less perfectly structured in composites containing ChNFs. The 5CNC composite is a notable exception since it also showed higher crystallinity than the neat LPVA but a similar melting temperature. Ultimately, the difference in molecular weight for LPVA and HPVA appeared to have an important effect on the matrix crystallinity.

While not necessary for improving dispersion of CNCs, acetic acid was still added to the 5 wt% CNC PVA solutions in order to maintain uniformity across samples. In order to test the potential impact of the acetic acid on crystallinity, an additional test performed on 1 vol% acetic acid in neat HPVA sample showed a similar crystallinity of 38% in comparison to neat HPVA.

Table 3
Mechanical testing data for HPVA- and LPVA-based samples.

Sample name	Number of specimens	Modulus (MPa)	Tensile strength (MPa)	Strain at break (%)
Neat HPVA	7	5210 ± 1040	112 ± 15	17.9 ± 9.2
5CNC/HPVA	7	6540 ± 458	128 ± 11	14.3 ± 10.5
4CNC/1ChNF/HPVA	5	6420 ± 710	116 ± 13	18.6 ± 25.4
2.5CNC/2.5ChNF/HPVA	6	6570 ± 427	121 ± 31	3.3 ± 1.6
1CNC/4ChNF/HPVA	8	7430 ± 532	138 ± 7	7.0 ± 3.3
5ChNF/HPVA	9	6320 ± 763	130 ± 16	15.8 ± 9.6
Neat LPVA	4	5200 ± 428	115 ± 11	3.3 ± 1.3
5CNC/LPVA	6	6550 ± 487	107 ± 12	2.1 ± 0.4
4CNC/1ChNF/LPVA	4	5670 ± 235	80 ± 11	1.6 ± 0.3
2.5CNC/2.5ChNF/LPVA	6	7470 ± 258	120 ± 7	1.9 ± 0.1
1CNC/4ChNF/LPVA	6	6600 ± 557	108 ± 11	2.0 ± 0.3
5ChNF/LPVA	6	6510 ± 383	117 ± 4	2.4 ± 0.1

3.6. Mechanical testing

Mechanical testing data consisting of modulus, tensile strength, and strain at break were collected from the neat PVA and nanocomposite samples that contained various ratios of CNCs and ChNFs. These data are shown in Fig. 5 and Table 3. Bar graphs and box and whisker plots for the mechanical data are shown in Figs. S10 and S11. These figures also denote which sample sets had property differences that were statistically significant, as well as any outliers. Fig. 5a displays representative stress-strain curves of each of the HPVA-based samples. The samples selected for inclusion in this figure most closely approximated the average and/or median values for modulus, tensile strength, and strain at break for each sample set. All the nanocomposite samples were found to have statistically greater average values of modulus than that of the neat HPVA (Fig. S1), suggesting that the addition of cellulose- and/or chitin-based nanofillers at a 5 wt% loading caused an increase in resistance to deformation. Within this sample set, the highest modulus was observed for the 1CNC/4ChNF/HPVA nanocomposite. Additionally, the 5CNC and 5ChNF nanocomposite samples were shown to have statistically similar modulus values. This result appeared logical provided that CNCs have a reported elastic modulus around 50 GPa [55] compared to the slightly lower 41 GPa of crystalline regions of chitin [56]. The short length of the CNCs suggested there might not be a complete load transfer, possibly explaining the similar values between the two different nanofiller types despite the slightly higher modulus of CNCs.

The tensile strength data did not show that all of the composites had a higher tensile strength than the neat HPVA. Three composite samples were found to have tensile strength values that were greater than that of the neat HPVA by statistically significant amounts: 5CNC/HPVA, 1CNC/4ChNF/HPVA, and 5ChNF/HPVA, though these values were not statistically different from one another (Fig. S2). Furthermore, a previous study by Mok et al. (2017) compared tricomponent PVA composites containing cellulose and chitin in nanofiber form. Results showed certain ratios between cellulose and chitin had the largest moduli and tensile strength. The authors suggested this is the result of chitin nanofibers binding to themselves through hydrogen bonding, creating a high strength network, with the CNCs potentially enhancing interaction among chitin molecules and increasing the mechanical capabilities. The authors also suggested that above certain CNC loadings (particularly 1 wt%) agglomeration occurs between particles which generates weak points in the material, which could explain the relative decrease in mechanical properties with particular loadings [39]. Additionally, it is worth noting that while the 2.5CNC/2.5ChNF/HPVA data set overall performed similarly to the other nanofiller data sets, one sample experienced brittle failure without yield and is represented in Fig. S10 as an outlier.

Overall, the strain at break data showed that the composites had less ductility than the neat HPVA. Some samples experienced wide ranges of breaking strain values, which complicated the data analysis. The 4CNC/1ChNF/HPVA sample specifically experienced relatively uniform strain at break values except for one sample that extended up to 65% of its original length, thus skewing its distribution. Furthermore, statistical analysis showed that all samples except for this 4CNC/1ChNF/HPVA data set were statistically greater than the 2.5CNC/2.5ChNF/HPVA data set (Fig. S3). Generally, the mechanical property data indicated that the addition of nanofillers caused an increase in modulus and tensile strength with a simultaneous decrease in strain at break properties. This type of behavior has been found previously in other polymer nanocomposites [57–59] and was not unexpected at this nanoparticle loading.

For the LPVA-based materials, some similarities and some differences in the mechanical properties were observed relative to the corresponding HPVA-based materials. Representative stress–strain curves for the LPVA-based materials are shown in Fig. 5b. The stress–strain curves used in this figure were chosen in the same way as those used in Fig. 5a. All of the composites except the 4CNC/1ChNF/LPVA composite showed a statistically significant increase in modulus in comparison to the neat LPVA control, indicating that a 5 wt% loading of nanofillers caused an overall increase in resistance to deformation (Figs. S1 and S11). Neat HPVA and neat LPVA average modulus values were statistically similar with values of approximately 5200 MPa, and composites containing only one nanofiber (i.e. 5CNC or 5ChNF) were statistically similar to one another within the LPVA sample set and to the corresponding HPVA-based samples. However, the composites from the two different PVA sample sets with the highest modulus value did not have the same composition. The 2.5CNC/2.5ChNF/LPVA sample displayed a statistically significantly greater modulus average than the other LPVA samples. This sample had a different CNC/ChNF ratio than the HPVA-based composite with the highest modulus, which was 1CNC/4ChNF/HPVA. It was not clear why different combinations of nanofillers achieved the highest modulus value in different PVA polymers, while the composites containing only one type of nanofiber were more similar. This difference suggested that the molecular weight of polymer chains and entanglement density is a factor in the dispersion and interaction between CNCs and ChNFs.

While modulus was enhanced by the addition of nanofibers, the addition of CNCs, ChNFs, or combinations of these nanofibers did not improve the tensile stress. None of the composites had a statistically greater tensile strength than the neat LPVA. Additionally, the HPVA tensile strength values were higher than their corresponding LPVA values for all five of the nanofiller loadings by an average of approximately 20 MPa, with all but the 2.5CNC/2.5ChNF sample being statistically greater (Fig. S2).

For strain at break, the neat LPVA had the highest value, similar to the HPVA-based materials. The strain at break values for the LPVA nanocomposites appeared to have smaller distributions and standard deviations in comparison to the HPVA nanocomposites, though most

were not statistically different from one another. One explanation could be related to how the LPVA samples tended to break at their tensile strength value, while the HPVA tended to yield and break after the yield point. Therefore, differences in their mechanical properties in this regard could be related to characteristics in the matrix polymer such as the length of the polymer chains, entanglement density, and the ease of generating fracture points in the shorter chains as they are pulled apart. Four of six HPVA-based samples had a statistically greater strain at break value in comparison to their LPVA counterpart: 5CNC, 1CNC/4ChNF, 5ChNF, and neat PVA. Only the 4CNC/1ChNF/HPVA and 2.5CNC/2.5ChNF/HPVA data sets did not provide a statistically greater value than those given in the LPVA samples.

As a comparison to these mechanical property results, a previous study examined cellulose/chitin composite gels and films generated by combining the two biomaterials dissolved in ionic liquids and analyzed various properties of the bicomponent films [60]. Even though these results were for gels and films produced with cellulose and chitin solutions as opposed to the nanoscale fibers discussed here, they provide some context for the types of interactions that could occur. The mechanical properties determined by this previous study showed a progressive increase in relative modulus as the ratio of chitin to cellulose increased, which agreed with the trends observed here for HPVA-based samples. In addition, this trend agreed somewhat with the LPVA data (there was an increase in modulus as ChNF was added with exception to the 1CNC/4ChNF/LPVA sample). Lastly, it is worth noting that the sample with the lowest modulus average for combined nanofillers was the same for each molecular weight at weight loadings of 4% CNC and 1% ChNF (4CNC/1ChNF/HPVA and 4CNC/1ChNF/LPVA). While approximate, the 4CNC/1ChNF ratio is similar to that of the charge neutral ratio presented in the zeta-potential of Fig. 2. From this correlation, it is possible that charge-driven association of CNCs and ChNFs leads to less effective mechanical reinforcement through reduced nanofiber-polymer interactions. In contrast, composites containing CNC/ChNF ratios with unbalanced surface charges, specifically those with excess positive charge from excess ChNF content, were shown to have better mechanical properties than singular nanofiller composites containing only CNCs or only ChNFs.

This potential for charge-driven association was also alluded to in the FTIR results. While it was difficult to separate different contributions to the -OH stretching peak, the 1CNC/4ChNF/HPVA and 4CNC/1ChNF/HPVA samples possessed the highest and lowest mechanical properties of the HPVA-based composites, respectively, which correlated roughly to their -OH peak intensities. Similarly, the LPVA-based material with the largest modulus and tensile strength, 2.5CNC/2.5ChNF/LPVA, corresponded to the highest intensity –OH stretching peak, while the nanocomposite material with the lowest mechanical performance, 4CNC/1ChNF/LPVA, corresponded to the lowest intensity peak for a nanocomposite.

Aside from component interactions, the influence of matrix crystallinity on mechanical properties was also examined. Overall, the trends in matrix crystallinity did not correlate to the measured modulus and tensile strength values. For both molecular weights, the CNC/ChNF ratios that possessed the highest moduli and tensile strength did not correlate to the largest crystallinity value, so the crystallinity did not appear to be the most important factor influencing mechanical performance. However, while experimental error in the crystallinity values was larger for HPVA composites containing ChNFs than the 5CNC composite and neat HPVA, the 4CNC/1ChNF/HPVA sample had the lowest reported crystallinity of the HPVA-based composites, which corresponded to its relatively low mechanical performance, so the matrix crystallinity could not be completely discounted as a contributing factor in this composite's mechanical properties. Considering the mechanical testing, FTIR, and MDSC data together, the results consistently suggested a lower performance for the composites containing the nanofillers at the CNC/ChNF ratio that was closest to a balanced charge ratio as shown by the zeta potential measurements.

The improved mechanical performance for composites containing other CNC/ChNF ratios was not as easily deduced from these results and was likely a result of differences in nanofiller distribution and dispersion, which were influenced by the amounts of each nanofiller in the composite as well as the molecular weight of the polymer matrix.

While the amount of research available on tricomponent composites utilizing cellulose- and chitin-based nanomaterials is limited, the enhancement in properties presented in this paper compare favorably to results from recent literature utilizing one of the nanomaterials. Roohani et al. (2008) demonstrated that roughly a 25% increase in modulus and a 18% increase in tensile strength can be achieved with 6 wt% loadings of CNCs in HPVA, which agrees with the 26% and 14% increase in those respective properties found for 5CNC/HPVA in the current study. Additionally, the highest achieved properties from this earlier study from 12 wt% CNCs experienced roughly a 50% increase in modulus and 23% increase in tensile strength, which is comparable to the 1CNC/4ChNF/HPVA sample set that possessed an average increase of 43% for modulus and 23% for tensile strength while utilizing less than half of the nanofillers [9]. For comparisons to LPVA, a study by Fortunati et al. (2013) found a decrease in modulus for 1, 3, and 5 wt% CNC loadings, with an increase of 46% for 10 wt% CNCs. Our study found a 26% increase in modulus for the 5CNC/LVPA samples compared to neat LPVA, while the 43% increase in modulus measured for 2.5CNC/2.5ChNF/LPVA is comparable to the 10 wt% loadings of Fortunati's study [41]. For comparing to chitin-based nanofillers, the more common acid hydrolysis of chitin to produce chitin nanowhiskers (ChNWs) has previously shown approximately a 36% and 28% increase in modulus and tensile strength, respectively, compared to neat PVA for 5 wt% ChNWs [36]. These increases are greater than that achieved by 5ChNF/HPVA (21% and 16% increase in modulus and tensile strength, respectively) and 5ChNF/LPVA (25% and 2% increase in modulus and tensile strength, respectively), though this discrepancy may be the result of the shorter, more crystalline chitin nanomaterials. However, the same study reported a 46% increase in modulus for 10 wt% ChNWs that is consistent with the modulus increases provided by 1CNC/4ChNF/HPVA and 2.5CNC/2.5ChNF/LPVA, in addition to a tensile strength increase of 22% consistent with the 23% increase provided by 1CNC/4ChNF/HPVA. Overall, composites containing certain CNC/ChNF ratios possessed greater values of modulus and tensile strength than composites containing only one type of nanofiller. Many of these differences were statistically significant, providing evidence of synergistic interactions between CNCs and ChNFs.

4. Conclusions

The ability to modulate properties of water-soluble polymers like PVA by creating nanocomposites with mixtures of cellulosic and chitinous nanomaterials is relatively underexplored. Traditionally nanocomposites are constructed utilizing one nanomaterial as a filler. However, this paper draws attention to the possibility of allowing for further tuning of the mechanical properties through the introduction of a second nanofiller. Materials generated in this study showed an overall increase in stiffness, tensile strength, and thermal degradation in both HPVA and LPVA systems. Furthermore, CNC/ChNF mixtures at certain ratios were able to more effectively reinforce PVA than CNCs or ChNFs alone. Films containing nanofillers also experienced a small shift in delay of polymer degradation. Properties appeared to be somewhat correlated to the PVA crystallinity, but with different trends observed in the different molecular weight samples containing ChNFs. While previous studies have shown that lower nanofiller loadings within polymers tended to correlate with higher strain at break values compared to high nanofiller loadings,[61,62] the reduction in strain at break for 5 wt% nanofiller samples compared to the neat PVA samples in this study provides a point to be improved in future work. Zeta-potential and titration testing suggested that this behavior could be linked to charge-driven association of ChNFs and CNCs near ratios of ChNF and CNC that

achieve neutrality. This paper provides evidence that there are some physical and/or chemical interactions the nanofillers and polymer matrix that are generating properties that extend beyond that of what can be achieved with a single nanofiller when nanofiller ratios are chosen to avoid complex formation. The combination of stiff, renewable biomaterials with the barrier properties of PVA could potentially be applied to industries looking to utilize a biodegradable packaging material that provides resistance to tear and air permeation.

This paper opens questions about how polymer nanocomposites might be further altered to allow for additional customizability through the addition of a second nanofiller. How these materials behave when utilizing higher weight percent additions of CNCs, ChNFs, or any other nanocomposite are additional avenues for study. Furthermore, the effects these fillers may have on other polymers and in other composite forms, such as hydrogels and aerogels, may provide additional information on their interactions with one another and surrounding polymer matrix. The materials generated in this study demonstrated that three-component polymer nanocomposites utilizing renewable nanofillers at relatively low loadings showed enhanced capabilities in modulus, tensile strength, and thermal degradation, and this general methodology has the potential to be used in applications necessitating a level of customizability.

Acknowledgements

Appendix A. Supplementary data

Supplementary data to this article can be found online at https://doi.org/10.1016/j.compositesa.2018.10.028.

References

[1] Abdul Khalil HPS, Bhat AH, Ireana Yusra AF. Green composites from sustainable cellulose nanofibrils: a review. Carbohydr Polym 2012;87(2):963–79.
[2] Raquez JM, Deléglise M, Lacrampe MF, Krawczak P. Thermosetting (bio)materials derived from renewable resources: a critical review. Prog Polym Sci 2010;35(4):487–509.
[3] Flieger M, Kantorová M, Prell A, Řezanka T, Votruba J. Biodegradable plastics from renewable sources. Folia Microbiol 2003;48(1):27.
[4] Siracusa V, Rocculi P, Romani S, Rosa MD. Biodegradable polymers for food packaging: a review. Trends Food Sci Technol 2008;19(12):634–43.
[5] Jayakumar R, Menon D, Manzoor K, Nair SV, Tamura H. Biomedical applications of chitin and chitosan based nanomaterials—A short review. Carbohydr Polym 2010;82(2):227–32.
[6] Jorfi M, Foster EJ. Recent advances in nanocellulose for biomedical applications. J Appl Polym Sci 2015;132(14). n/a-n/a.
[7] de Leiris JP. Cellulose packaging films for packaging soft cheeses. Google Patents; 1981.
[8] Srinivasa PC, Tharanathan RN. Chitin/chitosan — safe, ecofriendly packaging materials with multiple potential uses. Food Rev Int 2007;23(1):53–72.
[9] Roohani M, Habibi Y, Belgacem NM, Ebrahim G, Karimi AN, Dufresne A. Cellulose whiskers reinforced polyvinyl alcohol copolymers nanocomposites. Eur Polym J 2008;44(8):2489–98.
[10] Hussain F, Hojjati M, Okamoto M, Gorga RE. Review article: polymer-matrix nanocomposites, processing, manufacturing, and application: an overview. J Compos Mater 2006;40(17):1511–75.
[11] Moon RJ, Martini A, Nairn J, Simonsen J, Youngblood J. Cellulose nanomaterials review: structure, properties and nanocomposites. Chem Soc Rev 2011;40(7):3941–94.
[12] Eichhorn SJ. Cellulose nanowhiskers: promising materials for advanced applications. Soft Matter 2011;7(2):303–15.
[13] Favier V, Canova GR, Cavaillé JY, Chanzy H, Dufresne A, Gauthier C. Nanocomposite materials from latex and cellulose whiskers. Polym Adv Technol 1995;6(5):351–5.
[14] Battista OA. Hydrolysis and crystallization of cellulose. Ind Eng Chem 1950;42(3):502–7.
[15] Immergut EA, Rånby BG. Heterogeneous acid hydrolysis of native cellulose fibers. Ind Eng Chem 1956;48(7):1183–9.
[16] Ben Azouz K, Ramires EC, Van den Fonteyne W, El Kissi N, Dufresne A. Simple method for the melt extrusion of a cellulose nanocrystal reinforced hydrophobic polymer. ACS Macro Lett 2012;1(1):236–40.
[17] Orr MP, Shofner ML. Processing strategies for cellulose nanocrystal/polyethylene-co-vinyl alcohol composites. Polymer 2017;126(Supplement C):211–23.
[18] Azizi Samir MAS, Alloin F, Dufresne A. Review of recent research into cellulosic whiskers, their properties and their application in nanocomposite field. Biomacromolecules 2005;6(2):612–26.
[19] Hietala M, Sain S, Oksman K. Highly redispersible sugar beet nanofibers as reinforcement in bionanocomposites. Cellulose 2017;24(5):2177–89.
[20] Oksman K, Aitomäki Y, Mathew AP, Siqueira G, Zhou Q, Butylina S, et al. Review of the recent developments in cellulose nanocomposite processing. Compos A 2016;83:2–18.
[21] Jirawut J, Ratana R, Pitt S. Fabrication of α-chitin whisker-reinforced poly(vinyl alcohol) nanocomposite nanofibres by electrospinning. Nanotechnology 2006;17(17):4519.
[22] Ravi Kumar MNV. A review of chitin and chitosan applications. React Funct Polym 2000;46(1):1–27.
[23] Sripapayo J, Supaphol P, Blackwell J, Rujiravanit R. Preparation and characterization of α-chitin whisker-reinforced poly(vinyl alcohol) nanocomposite films with or without heat treatment. Polymer 2005;46(15):5637–44.
[24] Hamed I, Özogul F, Regenstein JM. Industrial applications of crustacean by-products (chitin, chitosan, and chitooligosaccharides): a review. Trends Food Sci Technol. 2016;48:40–50.
[25] Gopalan Nair K, Dufresne A. Crab shell chitin whisker reinforced natural rubber nanocomposites. 1. processing and swelling behavior. Biomacromolecules 2003;4(3):657–65.
[26] Wu J, Zhang K, Girouard N, Meredith JC. Facile route to produce chitin nanofibers as precursors for flexible and transparent gas barrier materials. Biomacromolecules 2014;15(12):4614–20.
[27] Girouard N. Cellulose nanocrystal thermoset composites: a physical and chemical route to improving dispersion and mechanical properties. Georgia Tech Theses Dissert 2015.
[28] Azizi S, Ahmad MB, Ibrahim NA, Hussein MZ, Namvar F. Preparation and properties of poly(vinyl alcohol)/chitosan blend bio-nanocomposites reinforced by cellulose nanocrystals. Chin J Polym Sci. 2014;32(12):1620–7.
[29] Baker MI, Walsh SP, Schwartz Z, Boyan BD. A review of polyvinyl alcohol and its uses in cartilage and orthopedic applications. J Biomed Mater Res, Part B 2012;100B(5):1451–7.
[30] Peresin MS, Habibi Y, Zoppe JO, Pawlak JJ, Rojas OJ. Nanofiber composites of polyvinyl alcohol and cellulose nanocrystals: manufacture and characterization. Biomacromolecules 2010;11(3):674–81.
[31] Nijenhuis KT. Poly(vinyl alcohol) Thermoreversible Networks: Viscoelastic Properties and Structure of Gels. Berlin Heidelberg: Berlin, Heidelberg:Springer; 1997. p. 37–66.
[32] Hassan CM, Peppas NA. Structure and applications of poly(vinyl alcohol) hydrogels produced by conventional crosslinking or by freezing/thawing methods. Adv Polym Sci 2000;153:37–65.
[33] Lee JS, Choi KH, Ghim HD, Kim SS, Chun DH, Kim HY, et al. Role of molecular weight of atactic poly(vinyl alcohol) (PVA) in the structure and properties of PVA nanofabric prepared by electrospinning. J Appl Polym Sci. 2004;93(4):1638–46.
[34] Peng Z, Kong LX. A thermal degradation mechanism of polyvinyl alcohol/silica nanocomposites. Polym Degrad Stab. 2007;92(6):1061–71.
[35] Voronova MI, Surov OV, Guseinov SS, Barannikov VP, Zakharov AG. Thermal stability of polyvinyl alcohol/nanocrystalline cellulose composites. Carbohydr Polym. 2015;130:440–7.
[36] Uddin AJ, Fujie M, Sembo S, Gotoh Y. Outstanding reinforcing effect of highly oriented chitin whiskers in PVA nanocomposites. Carbohydr Polym 2012;87(1):799–805.
[37] Araki J, Yamanaka Y. Anionic and cationic nanocomposite hydrogels reinforced with cellulose and chitin nanowhiskers: effect of electrolyte concentration on mechanical properties and swelling behaviors. Polym Adv Technol 2014;25(10):1108–15.
[38] Jalal Uddin A, Araki J, Gotoh Y. Toward, "Strong" green nanocomposites: polyvinyl alcohol reinforced with extremely oriented cellulose whiskers. Biomacromolecules 2011;12(3):617–24.
[39] Mok CF, Ching YC, Muhamad F, Abu Osman NA, Singh R. Poly(vinyl alcohol)-α-chitin composites reinforced by oil palm empty fruit bunch fiber-derived nanocellulose. Int J Polym Anal Charact 2017;22(4):294–304.
[40] Mark JE. Polymer Data Handbook. Oxford University Press; 1999.
[41] Fortunati E, Puglia D, Monti M, Santulli C, Maniruzzaman M, Kenny JM. Cellulose nanocrystals extracted from okra fibers in PVA nanocomposites. J Appl Polym Sci 2013;128(5):3220–30.
[42] Socrates G. Infrared and Raman Characteristic Group Frequencies: Tables and Charts. Wiley; 2001.
[43] Sudhamani SR, Prasad MS, Udaya Sankar K. DSC and FTIR studies on Gellan and Polyvinyl alcohol (PVA) blend films. Food Hydrocolloids 2003;17(3):245–50.
[44] Gu Q, Trindle C, Knee JL. Communication: Frequency shifts of an intramolecular hydrogen bond as a measure of intermolecular hydrogen bond strengths. J Chem Phys 2012;137(9):091101.
[45] Lee YM, Kimt SH, Kimt SJ. Preparation and characteristics of β-chitin and poly (vinyl alcohol) blend. Polymer 1996;37(26):5897–905.

[46] Petersson L, Kvien I, Oksman K. Structure and thermal properties of poly(lactic acid)/cellulose whiskers nanocomposite materials. Compos Sci Technol 2007;67(11):2535–44.

[47] Pracella M, Haque MM-U, Puglia D. Morphology and properties tuning of PLA/cellulose nanocrystals bio-nanocomposites by means of reactive functionalization and blending with PVAc. Polymer 2014;55(16):3720–8.

[48] Marten FL. Vinyl Alcohol Polymers. Encycl Polym Sci Technol: John Wiley & Sons, Inc.; 2002.

[49] Schick C. Differential scanning calorimetry (DSC) of semicrystalline polymers. Anal Bioanal Chem 2009;395(6):1589.

[50] Strawhecker KE, Manias E. Structure and properties of poly(vinyl alcohol)/Na + montmorillonite nanocomposites. Chem Mater. 2000;12(10):2943–9.

[51] Wang L-Y, Wang M-J. Removal of heavy metal ions by poly(vinyl alcohol) and carboxymethyl cellulose composite hydrogels prepared by a freeze-thaw method. ACS Sustain Chem Eng 2016;4(5):2830–7.

[52] Mahanta N, Teow Y, Valiyaveettil S. Viscoelastic hydrogels from poly(vinyl alcohol)-Fe(iii) complex. Biomater Sci. 2013;1(5):519–27.

[53] Hojo N, Shirai H, Hayashi S. Complex formation between poly(vinyl alcohol) and metallic ions in aqueous solution. J Polym Sci, Polym Symp 1974;47(1):299–307.

[54] Samaddar P, Sen K. Anion induced gelation in polyvinyl alcohol: a probe for metal ion speciation studies. J Sol-Gel Sci Technol 2015;73(2):389–95.

[55] Xu S, Girouard N, Schueneman G, Shofner ML, Meredith JC. Mechanical and thermal properties of waterborne epoxy composites containing cellulose nano-crystals. Polymer 2013;54(24):6589–98.

[56] Nishino T, Matsui Ryousuke. Nakamae, Katsuhiko. Elastic modulus of the crystal-line regions of chitin and chitosan. J Polym Sci, Part B: Polym Phys 1999;37(11).

[57] Fornes TD, Yoon PJ, Keskkula H, Paul DR. Nylon 6 nanocomposites: the effect of matrix molecular weight. Polymer 2001;42(25):09929–9940.

[58] Chazeau L, Cavaillé JY, Canova G, Dendievel R, Boutherin B. Viscoelastic properties of plasticized PVC reinforced with cellulose whiskers. J Appl Polym Sci. 1999;71(11):1797–808.

[59] Qian D, Dickey EC, Andrews R, Rantell T. Load transfer and deformation me-chanisms in carbon nanotube-polystyrene composites. Appl Phys Lett. 2000;76(20):2868–70.

[60] Takegawa A, M-a Murakami, Kaneko Y. Kadokawa J-i. Preparation of chitin/cel-lulose composite gels and films with ionic liquids. Carbohydr Polym. 2010;79(1):85–90.

[61] Paralikar SA, Simonsen J, Lombardi J. Poly(vinyl alcohol)/cellulose nanocrystal barrier membranes. J Membr Sci. 2008;320(1):248–58.

[62] Wu CL, Zhang MQ, Rong MZ, Friedrich K. Tensile performance improvement of low nanoparticles filled-polypropylene composites. Compos Sci Technol. 2002;62(10):1327–40.